Journal of Healthcare Informatics Research (2020) 4:151–173
https://doi.org/10.1007/s41666-020-00067-3

RESEARCH ARTICLE

Fully Automated Approach for Early Detection of Pigmented Skin Lesion Diagnosis Using ABCD

Mai S. Mabrouk, et al. *[full author details at the end of the article]*

Received: 18 July 2019 / Revised: 20 November 2019 / Accepted: 10 January 2020 /
Published online: 3 March 2020

Abstract

Computerized analysis of pigmented skin lesions (PSLs) is a lively space of survey that dates back over 25 years. Recently, different automated computer-based systems stand to be a helpful tool. Physicians' usage for ABCD worldwide as the main tool of diagnosis and self-examination make it the common reference for different skin cancer diagnosis models. This system is comprised of the main four key warning signs of the ABCD model that can be detected by visual inspection and more accurately identified by the automated system to diagnose melanoma. Based on the image area identified as PSL, through pre-processing and segmentation step, the features will then be detected regarding ABCD rule. According to what ABCD stands for, the proposed study extracts Asymmetry, Border and Color features, in addition to various parameters introduce parameter "D." Finally, as the worldwide definition of ABCD rule of cancer diagnoses was discussed, this research also makes the final decision according to the Total Dermoscopic Score (TDS) Index, in addition to another three popular machine learning classifiers. ANN, SVM, and K-nearest neighbor were used for classification of the segmented lesions in addition to the traditional TDS. This research shows perfect results for calculating the ABCD score automatically, which reflects its viability. Different experiments developed in regard to features variety and different classification methods to reach 98.1%, 95%, and 98.75% classification accuracy when dermoscopic images were classified by TDS, Automatic ANN, and linear SVM, respectively, where the clinical images reached perfect accuracy 100% when classified by linear SVM, and very promising result 98.75% as per automatic ANN. This system considered to be the first promising digitalized system for traditional TDS regarding the achieved accuracy and using of a simple Graphical User Interface (GUI) to facilitate user easy use.

Keywords ABCD · Pigmented skin lesion · TDS · Differential structure

1 Introduction

Skin cancer is an aggressive tumor appeared on the most superficial layer of skin—skin epidermis—as PSLs. Most skin cancer lesions are not from pigmented melanocytes but from non-pigmented cells [1]. Thus, basal cell carcinoma (BCC) and squamous cell

carcinoma (SCC) are considered to be the most two popular skin cancers [1, 2]. Nevertheless, melanoma skin cancer (MSC) may be a less popular and more deadly carcinoma. It counts for less than 5% among the other two skin cancer types, but it leads to death with a high rate of 75% [2, 3]. However, melanoma is incurable in its developed phases and survival with melanoma increased from 49% (1950–1954) to 92% (1996–2003). This goes back to new technology as computer-aided diagnosis (CAD) algorithms for skin cancer can help increase early diagnosis and so successful treatment avoiding several treatment processes [4].

Despite the big tendency of skin cancer treatment in its early stage, it highly depends on the accuracy of the proposed automated system. Skin diseases are considered to be one of the most difficult diseases to have an accurate automatic diagnosis due to its different structure that varies among patients according to their different skin type. Initial methods have been developed to help dermatologist screening out melanoma started by dermoscopy that depends on simple materials, such as point of oil, microscope lens, and visual light epiluminescence microscopy (ELM). This was later developed into a fiber light instead of using oil for a clearer image. Besides visual inspection using ELM or fiber light, other diagnostic models were also invested to assist dermatologist deciding if the lesion is benign or malignant such as (i) 7-point check, (ii) Menzia scoring system, and (iii) the so-called ABCD-rule and (iv) pattern analysis [5, 6]. These diagnostic models have become reasonable to physicians, but it was not enough for a reliable, fast, and accurate diagnosis.

As computer technology started its revolution and it had been investigated in all life fields, many different methods were proposed for CAD of skin cancer that copes with the lake of standardization of visual inspection. Regarding the vulnerability of skin cancer and the complex texture of PLS, different features, structures, models, and classification methods are recommended for investing integrated and efficient diagnostic methods. ABCD diagnosis model is the one proposed through this study which requires implementation of different types of features and parameters to compute the outcome of each single ABCD standard. This model was characterized by the useful value that its features are easy patterns which are explained in a computer algorithm. Furthermore, information like the lesion symmetry or edge steepness at the contour is not like medical forms such as tissues and vessels. Also, the scoring account is complex to estimate without specific software. However, ABCD model is usually classified by the traditional calculating method Total Dermoscopic Value (TDV); recently famous artificial intelligence algorithms were also used for classification.

The main challenging task of biomedical engineers is to fully automate the physician's vision into simply using an automated system. Through this study, the ABCD model will be presented in a fully automated system using a graphic user interface for the easy usage of the system. In addition to simplicity of GUI, system shows high accuracy and perfect results with the different classification methods, whether it was applied on dermoscopic or clinical images. Best result was achieved for both image types when the most prominent features of each were classified by linear SVM, which reached 100% and 98.75 when applied on clinical and dermoscopic images respectively. System simplicity, accuracy, and database variability make it a very promising addition to the various studies which handled CAD for the sake of PSL diagnosis as mentioned through the next section.

The presented paper is arranged through five successive sections. First, the introduction section presented to clarify the ambiguities of terminology used in the literature. Second, an extensive review of the recent studies and systems performed for melanoma diagnosis is presented through a literature review. By the third and the fourth sections, materials used and methodologies of work are mentioned, respectively. Finally, the results achieved through the different approaches applied will be discussed through the fifth section, experimental results.

2 Related Work

There is a great size of researches inspired by imaging processing discipline attached to the handling of PSL diagnosis. The number of researches had risen every year to reach about 450 publications in the duration of 1984–2012 [7]. Through these years significant progress occurred, which also provides future directions for some feasibility studies and work regarding the value of this kind of application. The overall structure of all systems described in various papers is roughly the same. Mostly the difference lies in the number and types of classifiers used and in the acquisition and handling of samples. The aim of this section is to present a brief survey of some of these attempts and tries to evaluate general look on the result's achieved with different methods and algorithms from the old decade to this time.

Starting by 1992, Stoecker and Moss who implemented digital imaging algorithm to dermatology [8]. In 2001, Ganster et al. [9] presented an identification system for melanoma by 21 features including shape and radiometric features, as well as local and global parameters, which had been designed to analyze the skin cancer. This research has achieved a sensitivity of 87% with a specificity of 92% using K-nearest neighbor (KNN) as a classification method. Blum et al. [10] studied the ABCD, Menzies score, and 7-point check rule to classify the patients that suffered from melanocytic lesions, wherein system reached high accuracy level: Menzies scored 83.3%, while ABCD and 7-point check reached 78.1% and 88.1% respectively. In 2004, a CAD system of melanocytic lesions is established [11] to estimate 64 different analytical parameters and classified all 837 melanocytic lesions. In 2010 Amaliah et al. proposed the MSC diagnosis method for ABCD feature extraction with an accuracy of 85% [12].

In 2012, the melanoma diagnosis algorithm is created by texture analysis and recognized by artificial neural network (ANN) using 102 dermoscopic images with 92% accuracy [13]. In 2013, a CAD system is obtained to classify melanoma and melanocytic skin cancer by using clinical photographic images instead of using dermoscopic images in order to increase the flexibility and availability of this system [14]. Another research developed a system using the ABCD model for melanoma diagnosis [15] that based on image segmentation and analysis factors for qualitative and quantitative of skin cancer images. Thus, it started to be our purpose to test the effect of using different features like morphological, geometric, and texture features, each alone and together. By the end of 2014, we handled the effect of morphological features by using two different classifiers [16].

In 2015, Jain et al. presented a CAD algorithm for the detection of MSC using image processing techniques to discriminate normal skin from melanoma skin tumors [17]. In 2016, a fully automated CAD system for PSL is designed to extract the morphological

and texture features for developing the performance of the system with an accuracy of 96.25% and 97% for dermoscopic and clinical images respectively [18]. In 2017, another approach for PSL diagnosis is used Otsu segmentation as a preprocessing step and ABCD as a feature extraction step [19]. Some studies [20–22] are summarized the comparing results and sand nearly to the last results that recorded by skin cancer automatic diagnosis algorithms. Recently, the classification of different types of skin cancer images is implemented by deep neural networks [23, 24]. The following two sections will discuss in detail the different methods applied to extract the main features and the experimental results of the applied approaches.

3 Materials

The major target of this research is to recognize the valuable characteristics of PLS differential structure by image processing vision. Thus, out of all the new modalities used nowadays that facilitate the visualization of skin lesion structure [25, 26], this study is mainly applied on dermoscopic images and clinical images. Images acquired by dermoscopy and special camera resulted "dermoscopic image"; other type of image is "photographic or clinical image" acquired by conventional camera [26]. For the ease of system flexibility, availability, and cost reduction, the clinical image was preferred, while dermoscopic images are essential for its ability to clarify lesion differential structures, especially when applying the ABCD model for diagnosis. Figure 1 shows the difference between the two types of image.

3.1 Database

This study was applied to a database consisting of 320 images for various PLS with different risk categories. All images were arbitrarily examined from the skin malady books and specialists' centers (www.dermoscopic.blogspot.com/, www.dermoscopyatlas.com). Images were equitably partitioned to the two fundamental classes: 160 dermoscopic and clinical lesion images. To differentiate between malignant and benign lesions, every one of the utilized databases was randomly partitioned to 80 lesions of each. The dominant part of the dermoscopic images was selected from (http://www.ee.siue.edu/~sumbaug/Borders%20Complete/), and clinical images utilized for that design are broadly accessible in [27].

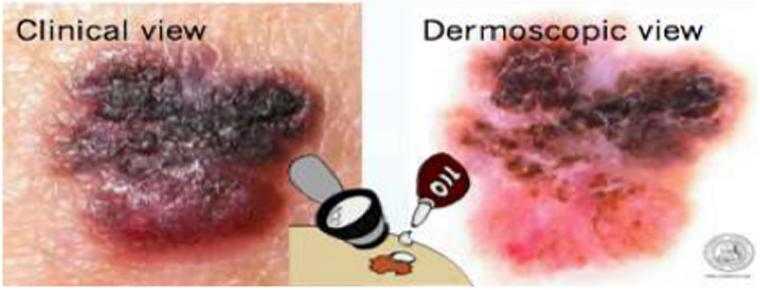

Fig. 1 Malignant melanoma image in clinical and dermoscopic view

3.2 Implementation

For fruitful diagnosis and a high computerized framework, a perfect visualization is fundamental that based on the implementation of ABCD rule on melanoma images by MATLAB version of 2010 on WINDOWS platform.

4 Methodology

The ABCD rule is a popular semi-quantitative method used to recognize dermoscopic criteria for melanoma diagnosis. It is a point-based framework where the physician allocates a score of each four categories. The categories are Asymmetry, Border, Color, and Differential structure or Diameter based on TDV [5]. To extract these four key warning signs from the desired lesion, some prior steps have to be performed. It starts with the pre-processing image for eliminating undesired artifacts and shading impacts. Then, a segmentation step is used to distinguish the lesion borders.

Then, ABCD features are calculated and the system classified and evaluated. This research describes all these steps, giving special attention to the different approaches for detecting the main parameters regarding the ABCD model. Thus, four main steps were mainly constructed to design an automated ABCD system. First, image pre-processing and segmentation applied to separate the region of interest. Second, A, B, C, and D features were extracted, followed by classification using TDV score and other different classifiers such as support vector machine (SVM), ANN, and KNN. Finally, the system performance was estimated according to sensitivity, specificity, and accuracy. Figure 2 shows a block diagram for the process.

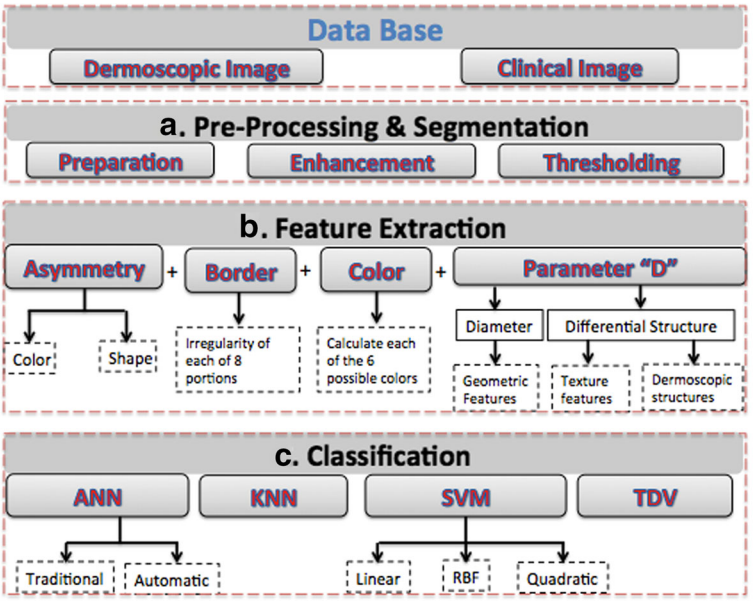

Fig. 2 Schematic representation for the proposed algorithm

4.1 Pre-processing and Segmentation

Efficient and meaningful features are highly focused on the accurate extraction of the lesion from the surrounding background. This process of separation has to go through the essential steps of pre-processing and preparation. The method applied here to segment the lesion was the same applied in our previous work through [16, 18]. First, the database was prepared where all images were resized and adjusted to the same scale. Then, image contrast was adjusted and filtered through the image enhancement step. Finally, the counter is clear enough to facilitate the separation process that was named as image thresholding. Figure 3 can simplify the performed steps for the ease of lesion segmentation.

4.2 Feature Extraction

The most important step toward designing the ABCD scoring system is to extract the main four features such as Asymmetry (A), Border (B), Color (C), and Diameter (D).

4.2.1 Asymmetry (A)

Feature (A) represents the tumor degree of asymmetry. Melanoma generally has more asymmetry shape and color than that of the benign nevus. For that reason, numerical indices about asymmetry are calculated regarding both tumor shape and color. The image is divided by two perpendicular axes to four regions; then, the symmetry is inspected across *x*- and *y*-axis intersecting at the centroid of the tumor. If the image shows asymmetric features on both axes according to color and shape, the asymmetry outcome is 2. If there is asymmetry on one axis, the outcome is 1. If asymmetry is lost, the outcome is 0. So for shape and color, there can be a maximum of two points if it shows asymmetry through both axes. According to the previous definition of Asymmetry, the first step toward calculating it is to divide the segmented lesion into two

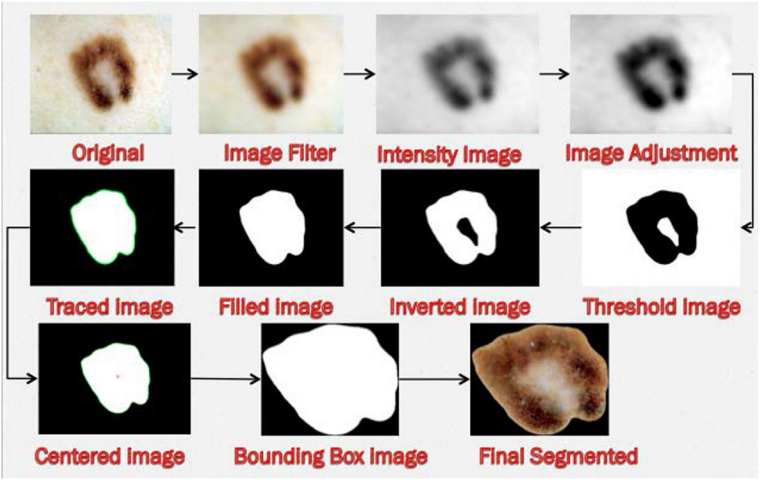

Fig. 3 Image segmentation steps for melanoma disease [18]

different axes and to compute or detect the symmetry of each half regarding the other; this process is designed as follows.

- Lesion division: Regarding the lesion centroid the central axis point was detected (X_c, Y_c). After that, the nearest point on the lesion boundary is detected, with respect to that of the central points. According to the four detected points, the lesion was divided into two horizontal and vertical halves as it was bisected by two 90 axes. Figure 4 illustrates the lesion four detected points and the divided tumor.
- Shape asymmetry calculation: After dividing the image vertically and horizontally, each half is compared with its adjacent. Measuring asymmetry is to mirror or reflect the mask about one of the principal axes and compute the non-overlapping part of the lesion. Asymmetry is defined as the near-axis of symmetry by computing the asymmetric index. The asymmetry index [28] compares the absolute area variances to the total area of the tumor shape that operated using Eq. (1). The asymmetry index then indicates perfect symmetry in case it is less than or equal 1.0; otherwise, it indicates asymmetry of that side if it is greater than 1. When the axes

$$AI = \frac{1}{2} \sum_{K=1}^{2} \frac{\Delta A_k}{A} \tag{1}$$

where:

ΔA is an overlapped region.
A is the total area of lesion.

- Color asymmetry calculation: The shape asymmetry is measured according to the binary mask of the lesion, but the same concept cannot be applied to color asymmetry. Consequently, each half is multiplied by the original image to yield the original lesion image divided by the same principle axes as shown in Fig. 5. Color asymmetry is measured by comparing the mean of the three-color components (μR, μG, μB) on both sides. According to this experiment, both sides considered symmetric in color if the difference between the three-color components is less than 0.05, otherwise considered to be asymmetric in color.

Accordingly, if both color and shape are symmetric, the "A" score is equal to "0." A score is equal to "1" if one axis was asymmetric in color or shape or each given that the other axis is totally symmetric. A score is equal to "2" if both axes were asymmetric in color or shape or each.

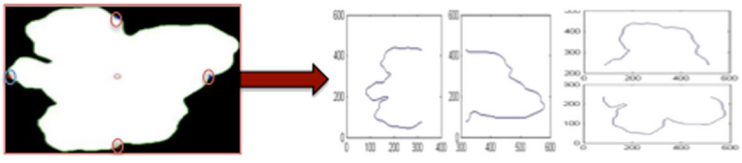

Fig. 4 The binary mask of the four detected points and the divided lesions

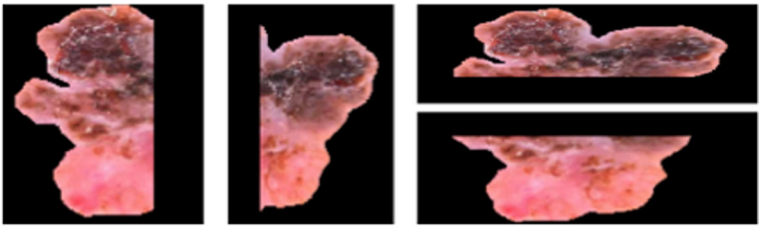

Fig. 5 The lesion colored in two halves

4.2.2 Border (B)

Melanoma tends to be blurred or irregular at the lesion border. There are a number of papers detailing the process of finding a measure of border irregularity. Two of the common ways for this measure are the compactness index and the fractal dimension methods [29]. The compactness index is the easiest to calculate, but in many cases, it is inappropriate to describe the shape of the border. Also, the fractal dimension does not act well to capture the difference between the uneven nature of the border on a small scale (wriggly) and the significant border irregularities [30]. As simple border parameter is a numerical value from 0 to 8, a lesion is partitioned into eight segments. The border of each segment is rated where the sharp boundary participates 1 score and the progressive boundary participates 0 score. Therefore, there can be a maximum of 8 points if all segments recorded to be blurred. Consequently, the border assessment process was designed in two steps; first divide the segment then evaluate it.

- Lesion division: To complete the lesion division process as described earlier, there are other two lines cut through the center, each of them at 45° inclined to horizontal. As a result of that operation, the tumor area was divided into eight regions with similar angles as shown in Fig. 6.
- Border calculation: After the border is divided into eight portions, that step is operated to measure rotation invariance or border irregularity, then analyzing the sharpness for each portion independently. The segment border is considered a digital signal searching for peaks by determining whether each value of the input signal is local minimum or maximum. Then, each element of data is compared with its adjoining values. If an element of data is bigger than both of its adjoining, it is a local peak and that segment considered to be irregular. If there are no local peaks, that element is an empty vector and so the segment is recorded to be the smooth border. This described method is actually very similar to the original diagnosis

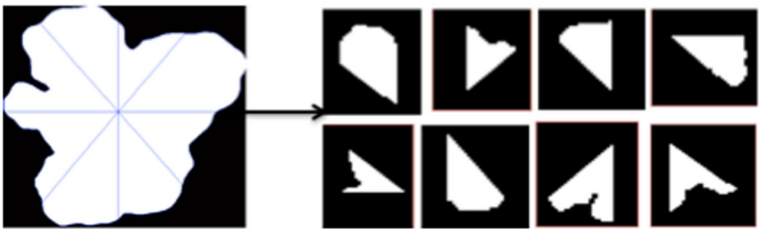

Fig. 6 Border division in two eight segments

method by human visual assessment. Each part is then graded for the blurriness, one point is awarded if the edge segment is blurry, and zero points are awarded if the edge segment is smooth. The points for each edge segment are totaled and used as one part of the diagnosis [19]. The maximum score that can be recorded is eight if local pecks or irregularities are recorded among the eight segments.

4.2.3 Color (C)

Measuring and extracting ABCD features and color variation features will be discussed in this section. Melanoma cells are commonly colorful like brown and black that based on the production of melanin pigment at various depths within the skin. The appearance of the emergence of color variations in situ sign is an important measurement in detecting malignant lesions [31]. The amount of different colors is positively correlated with the suspicion of melanoma [32]. Malignant tumor was typically recognized by three or more colors while 40% of melanomas were recognized by five or six colors. In other words, lesions that consist of more colors are seeming to be malignant. The lesion color variability was measured by computing the incidence of these typical hues inside a lesion segment.

- Color calculation: Physicians typically establish six special hues in skin lesions that include white, red, light brown (lBrown), dark brown (dBrown), blue-gray (bGray), and black. These basic colors are explained with the RGB color space in the range between 0.0 and 1.0 as shown in Table 1. The Euclidean distance D is calculated between the pixel color and the six colors as in Eq. (2) [33]. The counter of the nearest color is increased by $1/n$, where n is the number of pixels within the segmented area. The most obvious measure of similarity between two samples in the feature space is the distance between them. A color score is given by the sum of all values of the 6 color features so that a color maximum score is six if all colors were regarded.

$$D = \sqrt{(r-r1)^2 + (g-g1)^2 + (b-b1)^2} \tag{2}$$

For example, the first color white in the segmented lesion is given as the following numbers.

Table 1 Six special hues in skin lesions with the RGB color space

Color	Red	Green	Blue
White	1	1	1
Red	0.8	0.2	0.2
Light brown	0.6	0.4	0.25
Dark brown	0.4	0.26	0.13
Blue gray	0.2	0.6	1
Black	0	0	0

$$(\mathrm{r1}, \mathrm{g1}, \mathrm{b1}) = [1.0, 1.0, 1.0]$$

We obtain:

$$D = \sqrt{(r-1.0)^2 + (g-1.0)^2 + (b-1.0)^2}$$

If the considered pixel is white so the *D1* value supposes to be zero, which means that there is no difference observed.

4.2.4 Parameter (D)

D was not directly identified as the previously mentioned A, B, and C parameters, where previous literature describes it in two different ways. Some studies describe it as the tumor diameter [12], while other theories define it as a differential structure [34]. As it is crucial to know the effect and the different results of each, it was the target to study both ways and compare. The differential structures in the ABCD rule are only clear in dermoscopic images. Dermoscopic images mainly differ from those clinical images, as these images have magnified subsurface structures. As it was the intent of the proposed study to globalize the designed system to all image types, whether with highly magnified and detailed images (dermoscopic) or others acquired by a standard camera (clinical images), two methods are used to represent differential dermoscopic structures, the first, by calculating the differential structure in a traditional way (pigmented N.W, dot's, blue veil, Regression, and Irregular pigmentation), and the second through texture feature representation.

Diameter Melanoma diameter is larger than mole diameter; especially, it reaches to 6 mm. Previous theories present a scalar that represents the diameter of a circle as an indication of the probability of the malignancy of a PLS [35]. Calculating the diameter can be carried out somewhat easily, but the problem is that the 6 mm limit cannot be considered as a threshold, where according to the database, the scale is roughly known. Previous studies [12] assumed that if the wound is often irregular in form, diameter could be calculated by drawing a straight line from all border pixels to the opposite edge pixels among the center point and averaged. But this cannot be done practically. As long as different resolution and resizing operations are applied to the image, it is not quite accurate to depend on such a scalar definition to determine how large the lesion is. For that reason, it was preferred to define diameter through its geometric features.

According to the feature extracted in [16], the six most effective geometric features by the fisher score algorithm are used to compute the D score. Table 2 describes the six features used for dermoscopic and clinical images associated with the limit or threshold to specify melanoma according to experiments carried out through this study.

Differential Structure This section presents a process for early detection of skin cancer images. When dermoscopic pictures are applied, another set of diagnostic rules are needed. A group of specific features for differential structures has been observed [36]. The differential structure has six values to consider: irregular dots and globules, irregular pigment network, structure less areas, regression, pigmentation network, and

Table 2 Geometric features selection

Dermoscopic features	Limit
Equivalent Radius	110
Area	50,000
Perimeter	900
Roundness	0.75
Major Axis	300
Minor Axis	210

finally blue veil. Through this section, parameter "D" is represented by the sum of all values of the six variety features as shown in Fig. 7.

- Irregular pigmentation: Irregular pigmentation implies an irregular form of black or brown regions as displayed in Fig. 7. Previous studies used different color planes to study the differential structure present within the lesion region [38]. Considering that proposed color planes [16], the image undergoes the following steps to extract the required regions. In that study, it was observed that the irregular pigmentation was found in a lesion and was highly marked through the "L" plane of the Lab and "V" plane of HSV color space. Figure 8 shows a representation of that process.
- Irregular Dot's and globules: According to the lesion sample displayed in the image in Fig. 7, irregular Dots/Globules can be defined as black or brown regions in oval shapes with different sizes. Observing that the previous application for detecting irregular pigmented regions is concerned with all the pigmented regions regardless of their size or structure. The same process is applied to extract dots or globules that present in the lesion with respect to different density threshold adjustments. Irregular pigmented regions are considered irregular dot or globules, if their density is about 1/30000 of the total lesion area, and the lesion count down more than 30 regions. Figure 8 can identify the irregular pigmented region with the difference between dots and other structures considered irregular pigmentation.
- Blue veil: It is considered gray or blue regions that closed to irregular dots/globules [37]. It can be clearer on the image displayed in Fig. 7. Considering the seven color spaces discussed earlier [16], the HSV color space is the best describing many differential structures. As it can be used to describe irregular pigmentation through the "V" plane, it was also introduced describing the blue veil structure but through

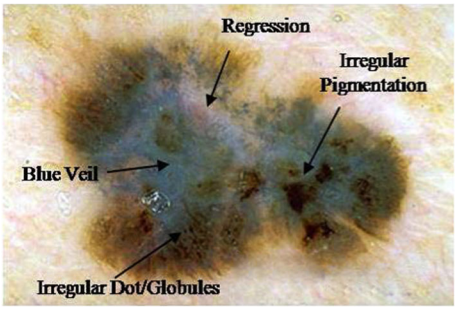

Fig. 7 Epiluminescence microscopy image of Melanoma [37]

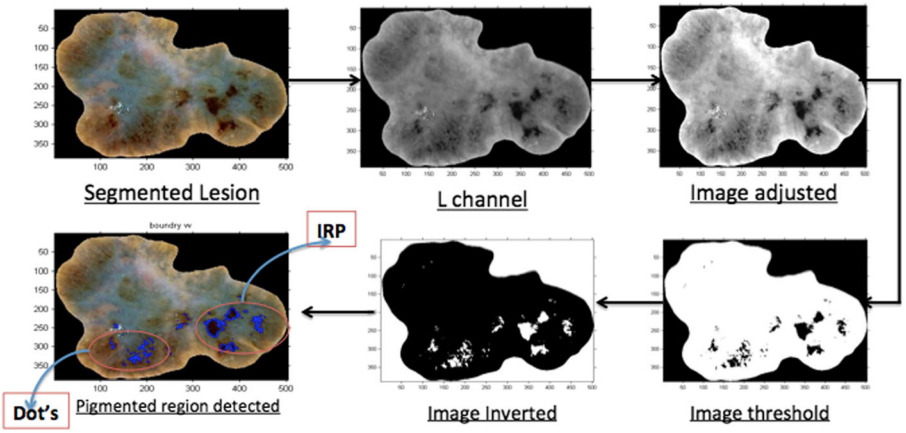

Fig. 8 Process of detecting irregular pigmented regions and Dot's

the "S" plane. The process applied to extract regression is the same applied for irregular pigmentation considering the color plane "S" instead of "V" and the density condition as well. Figure 9 shows an overview of the process for detecting blue veil. The blue veil could be detected as a present feature of the differential structure if the area of the region extracted within the ratio of (1/5000) of the total lesion area.

- Structure less: That structure considered being complementary to irregular pigmentation. It is also called hypopigmentation that performs as a widespread region of decreased pigmentation inside the normal pigmented lesion [39]. It was also mentioned by the same color space HSV but with different channels. According to the trails operated to find out the best plane describing light or structure less region as the same for the blue veil, it was noticed that "S" channel was the best to

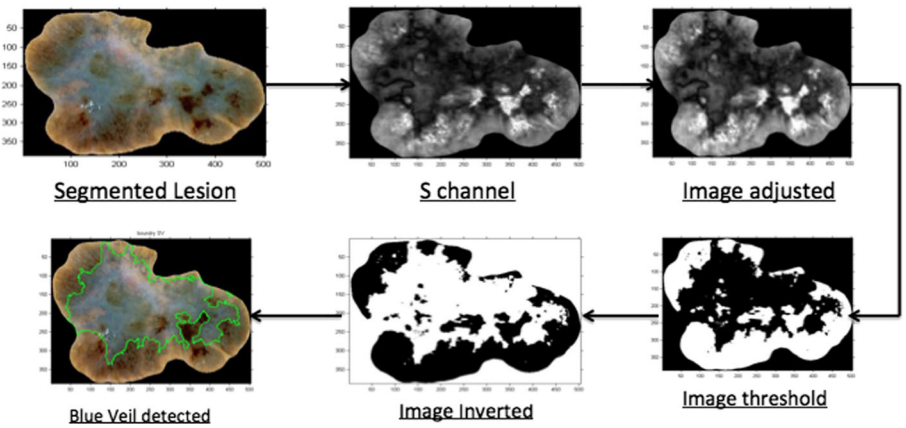

Fig. 9 Process of detecting Blue Veil

describe it. The process applied to define the di-pigmented region was near to that method applied for irregular pigmentation and blue veil but with minor changes. Figure 10 shows the process that the operation goes through to detect structure less region. Considering HSV color space the image undergoes the following steps to extract the required regions.

- Regression: These structures can be defined as a white scar that acts as irregularly distributed in the lesion [39], looking back to the lesion sample in Fig. 7. For that process, two different color spaces were introduced *YCbCr* and *Lab* color space, where both did cooperate to extract regression as follows. Figures 10 and 11 shows an overall description of the regression.
- Atypical pigmentation network: An atypical pigment network is defined as a black or brown region with irregular forms and thick streaks as shown in Fig. 12. The lesion network serves as a diagnostic feature, particularly if the network line and network allocation are references for this network. Regarding the search for the occurrence of pigmentation, texture spectral technique was designed [40].

The proposed algorithm applied to detect atypical pigmentation network consists of the following steps.

1. Convert from RGB to gray: At the first stage, the input segmented ELM color image is converted to intensity image (gray level).
2. Spectral technique: It is dependent on the Fourier transform, filtering, and inverse Fourier transform of the gray-level image as in Fig. 13.
3. Contrast adjustment: The image resulted from the Fourier transform is adjusted by means of histogram equalization.

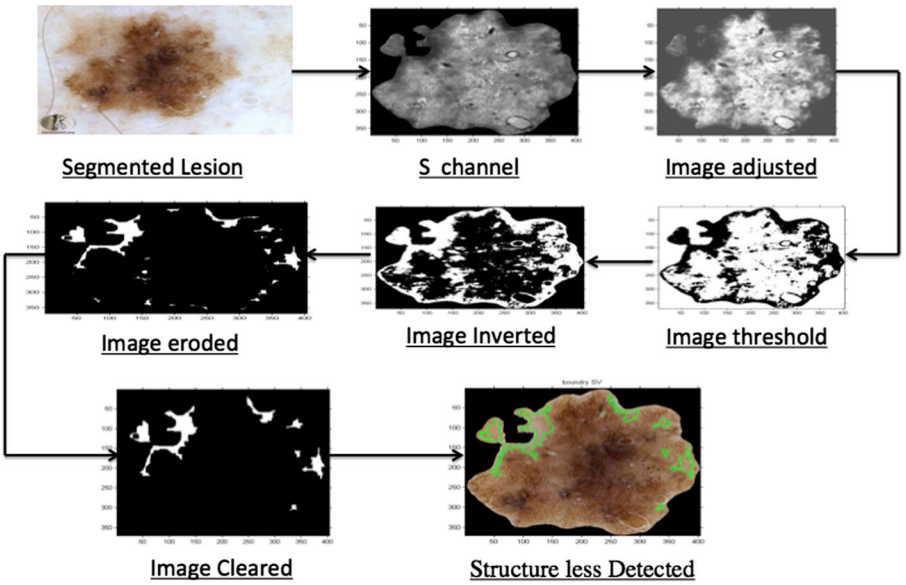

Fig. 10 Process of detecting Structure less using HSV color space

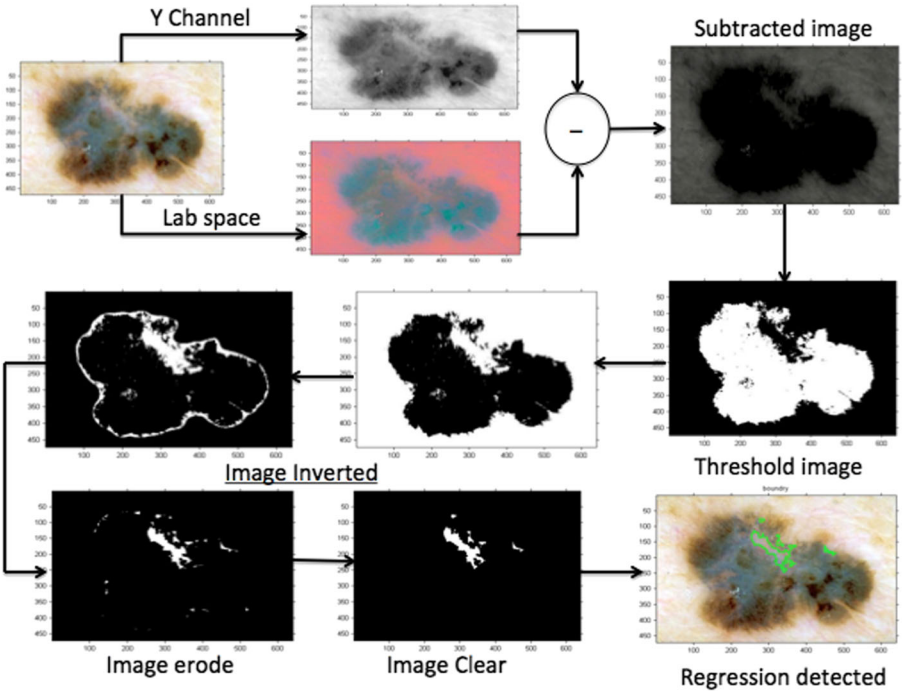

Fig. 11 Process of detecting Regression using luminance and Lab color space

4. Threshold: Otsu's threshold is applied to each pixel in the image as related to be the desired network or not.
5. Morphological operations: This deals with searching for streaks or points which can build the network structure. Morphological operations are introduced through four different steps, starting with skeleton operation to delete pixels on the edges of objects and it does not allow objects to fracture. It is followed by image double erosion, and finally, images cleared out of the small isolated points as shown in Fig. 14.
6. Regression density: The network might be a typical network that is not considered to be an indication for melanoma so that the density ratio was controlled between two threshold limits. If the pigmented network ratio calculated according to Eq. (3) results in a ratio between 25 and 35, this indicates the presence of an atypical

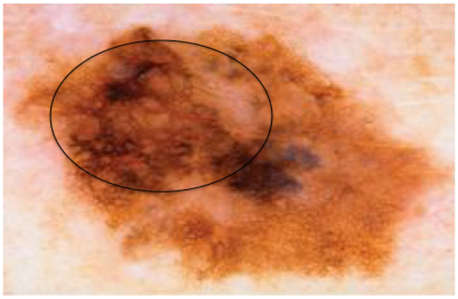

Fig. 12 Epiluminescence microscopy image by Atypical Pigmentation network

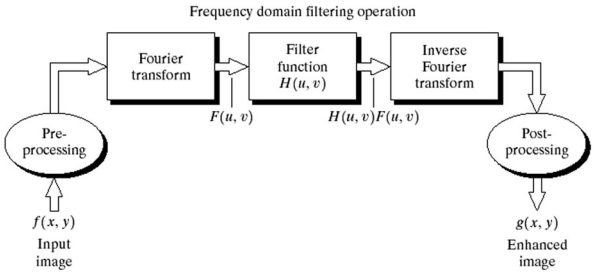

FIGURE 4.5 Basic steps for filtering in the frequency domain.

Fig. 13 Image filtration in the frequency domain

pigmentation network, and so the differential structure score is increment by 1; otherwise, it is ignored.

$$\text{PNR} = (\text{Area of the detected region}/\text{total area of the lesion}) \times 100 \qquad (3)$$

There are six dermoscopic structures that had been monitored through the PSL like irregular pigmentation, irregular dots, blue veil, structure less, regression, atypical pigmentation network. According to the procedures listed above to examine the differential structure of PSL, the presence of those structures depends mainly on the calculated density ratio and the threshold adjusted for it. It is serious to record that the values adjusted as a threshold for structure density were according to study experimental trails and were not previously listed.

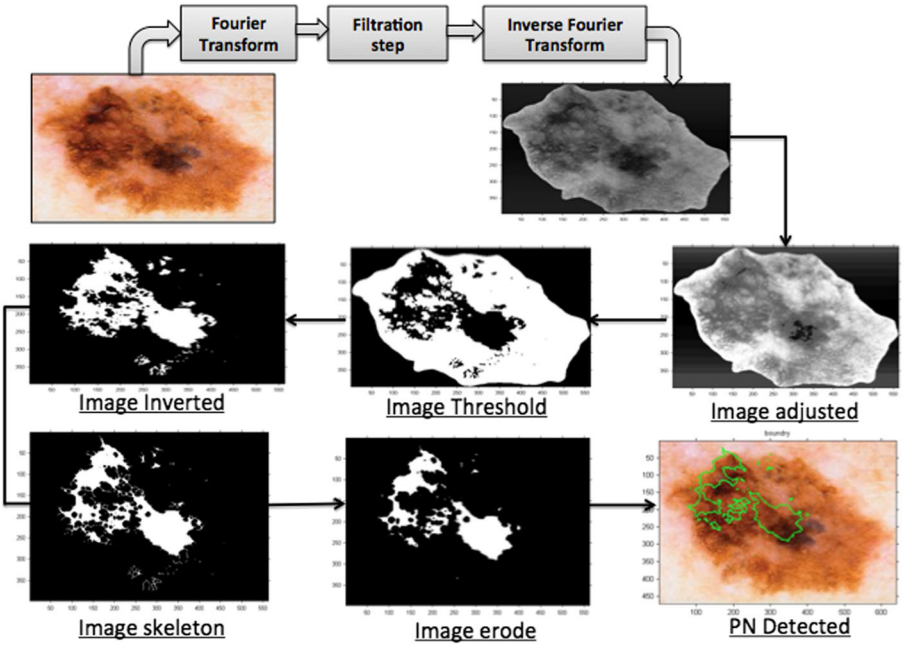

Fig. 14 Process of detecting Atypical Pigmentation N.W

Texture Features This kind of texture information is used for digital camera images. Thus, texture features are calculated on the gray scale image component in the segmented region by the Haralick-features. According to the 21 GLCM features previously mentioned through our research in [18], six features are selected based on the accuracy, which is previously mentioned as effective features. Considering the difference between the texture of dermoscopic and clinical images, different sets of features were selected for each type of image with different limits. Table 3 shows the different sets of features used for both types of data with their different limits.

4.3 Classification

All features are extracted with respect to the four main warning signs of the ABCD model. According to the main block diagram plotted in Fig. 1, the third step is to classify the introduced image to whether it is benign or malignant. The algorithms used in this study for classification are SVM, ANN, and KNN. All these classifiers were previously applied to the approaches introduced in [16, 18] for PSL diagnosis. Database of 160 PSL for each dermoscopic and clinical images were fairly divided into equal sets for both training and testing sets. Thus, the training set of dermoscopic and clinical images as well consist of 40 malignant lesions and 40 benign lesions. In addition to those classifiers, also the TDV scoring method was considered. Total dermoscopy value is also an efficient scoring method used for making a decision about the lesion when the ABCD model is applied. This section will discuss the four diagnosis methods performed for classifying the features extracted in the section above.

a) Artificial neural network: ANN is based on an artificial neuron that represents the signal sum and thresholds of biological neurons through mathematical calculations by activation function [41]. In this paper, the ANN classifier used two network topologies which have the same number of input/output and hidden nodes, with the same activation function but with different training techniques such as Automatic and Traditional ANN [16].
b) Support vector machine: SVM is based on the discovery of the best hyper-plane to differentiate all data in one class from the other class [42]. In this study, the SVM classifier used three different kernel functions [43] that are linear, quadratic, and RBF kernels.

Table 3 Texture features used for dermoscopic and clinical images

Dermoscopic	Limit	Clinical Features	Limit
Correlation	> 9.75 e-001	Max. probability	> 0.45
Energy	< 03	Energy	< 0.3
Entropy	< 1.65	Entopy	> 1.65
Sum Variance	> 0.45	Cluster prominence	> 100
Sum entropy	> 1.6	Sum entropy	> 1.5
Information measure of correlation 2	> 0.94	Information measure of correlation2	> 0.9

c) K-nearest neighbor: KNN is based on the separation between classes by K-sample neighbor that represent the distance closest computation between all data and class centers [44]. The restriction of the KNN classifier appears when using the large database.
d) Total Dermoscopic Value (TDV): The developed ABCD scoring software assigns points according to the four ABCD features as in Table 4. These points are weighted to produce total dermoscopy score (TDS), where an increased risk of lesion malignancy is defined when a higher score is gained. TDS can be calculated according to the "ABCD" rule by the formula presented in Eq. 4. It is noted that weight factor is a weight given to a data point to allocate it a lighter, or heavier, importance in a group.

$$\mathrm{TDS} = (\mathrm{A\ score} \times 1.3) + (\mathrm{B\ score} \times 0.1) + (\mathrm{C\ score} \times 0.5) + (\mathrm{D\ score} \times 0.5) \quad (4)$$

According to TDS equation, the following condition is considered for melanoma diagnosis [45]:

- TDV < 4.75 benign melanocytic lesion.
- 4.75 TDV < 5.45 suspicious lesion
- TDV > 5.45 lesion is melanoma.

According to the different classification algorithms proposed two different ANN approaches were introduced and another three SVM approaches were presented, in addition to K-NN and TDV scoring method. Data were classified by seven different methods, whose results will be discussed through the next section.

4.4 ABCD Model Presentation

The web-based GUI is used for displaying the images of melanoma lesion that based on GUIDE toolbox in MATLAB software by the implementation of the ABCD model. ABCD model is considered to be a separate automated diagnosis model for melanoma. It is interesting to design it by means of a GUI that makes it easy to visualize images and get data evaluation results. Figure 15 shows the ABCD model presented in the GUI

Table 4 Summary of ABCD features and their relative weights

Features	Definition	Score	Weight factor
Asymmetry	In 0,1 or 2 assess shape or color Asymmetry	0–2	*1.3
Border	Abrupt ending pattern at the periphery in 0–8 segments	0–8	*1.0
Color	Presence of up to six colors (white, red, light brown, dark brown, blue gray, black)	1–6	*0.5
Parameter D	Specified by three different methods, geometric features, texture features, and dermoscopic structure features.	1–6	*0.5

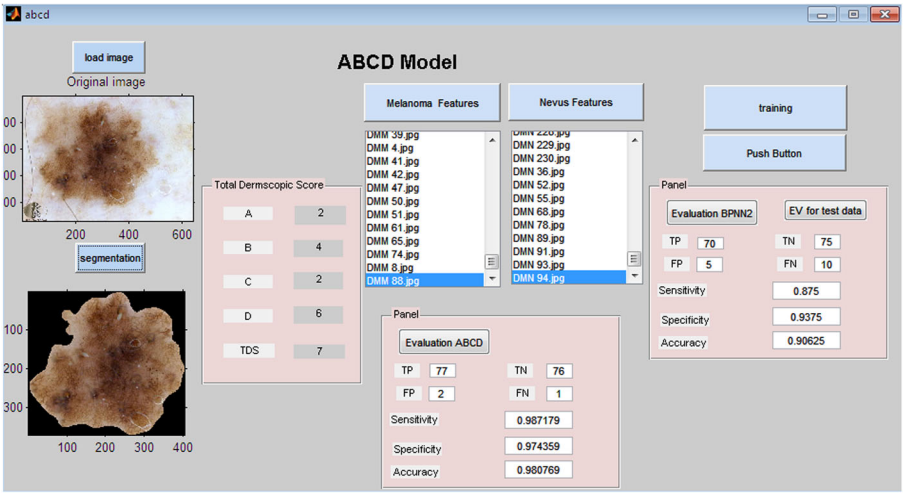

Fig. 15 ABCD Model in GUI form

form with annotation on each push button mentioning its function. It can also be seen in this figure that it can display the model evaluation by classifying the A, B, C, and D value using several classifiers presented through our study.

5 Results and Discussions

According to the ABCD model mentioned previously in Section 4, three different methods were proposed to calculate the parameter "D." The different methods used to represent "D" were six geometric features or six texture features where these methods can be applied to both dermoscopic and clinical images. The third method, which deals with the differential structures, can only be applied to the dermoscopic images. Thus, features used for ABCD Model analysis were represented by four features of Asymmetry, eight for Border, and six for color in addition to six different parameters representing "D." The ABCD model is supposed to be evaluated by the TDS. The six different classification methods were applied to the A, B, C, and D features to evaluate the effectiveness of using such parameters as features and compare their results with previous multiple model results from the work applied in [18].

5.1 Dermoscopic Images

5.1.1 Geometric Features

Area, Equivalent Radius, Perimeter, Roundness, Major Axis, and Minor Axis were the geometric features that represent parameter "D." These six features were combined with the basic A, B, and C features and classified by TDS and the other six classification algorithms. It was noted that the highest accuracy was achieved by classifying the ABCD features related to TDS and was 98.1%. Also, it was observed that the automated ANN well classifies the ABC and D features with an accuracy reaching 97.5%.

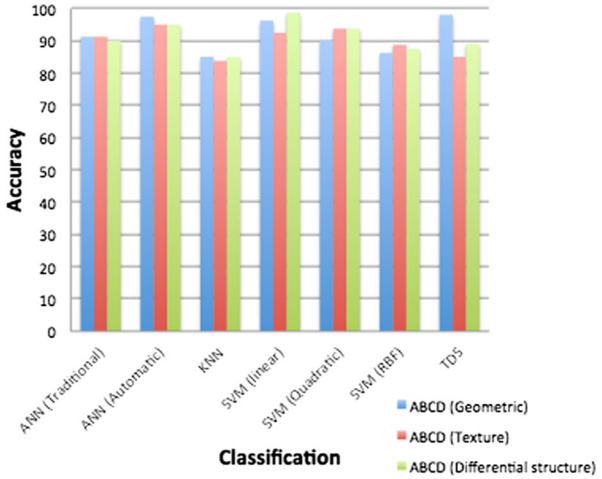

Fig. 16 Bar chart for the result achieved when applying the ABCD model of dermoscopic images

5.1.2 Texture Features

Correlation, Energy, Entropy, Sum variance, Sum entropy, and Information measure of correlation were the texture features that represent parameter "D." These six features were combined with the basic A, B, and C features and classified by TDS and other the other six classification algorithms. It was noted that the highest accuracy was achieved by classifying the ABCD features related to automatic ANN and was 95%.

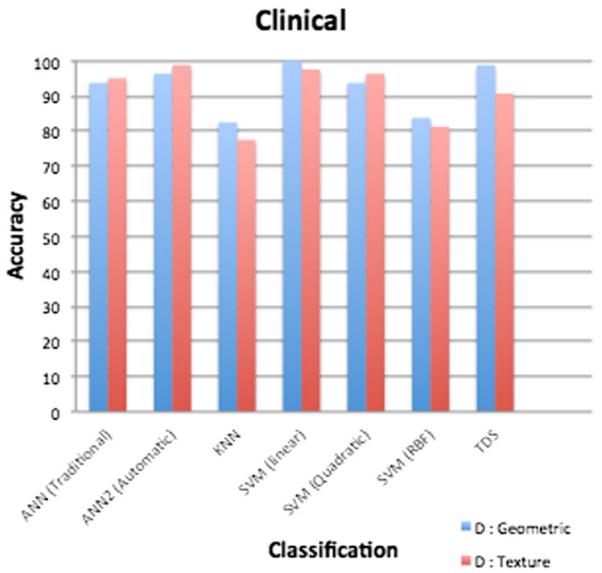

Fig. 17 Bar chart for the result achieved when applying the ABCD model on clinical images

5.1.3 Differential Structure

Irregular pigmentation, Dots/globules, Structure less, Regression, Blue Veil, and Atypical pigmentation network were the dermoscopic structures representing parameter "D." These six features were combined with the basic A, B, and C features and classified by TDS and the other six classification algorithms. The best accuracy was observed by classifying the ABC and D features according to linear kernel SVM, thus reaching 98.75%.

5.2 Clinical Images

5.2.1 Geometric Features

Area, Equivalent Radius, Perimeter, Roundness, Major Axis, and Minor Axis were the geometric features that represent parameter "D." These six features were combined with the basic A, B, and C features and classified by TDS and the other six classification algorithms. The linear Kernel function of SVM correctly classifies all test data and records perfect accuracy as a result of A, B, C, and D feature combination reaching 100%. It was also noted that a high accuracy was obtained by classifying the ABCD features related to TDS that record accuracy of 98.7%.

5.2.2 Texture Features

Maximum Probability, Energy, Entropy, Cluster Prominence, Sum entropy, and Information measure of correlation were the texture features that represent parameter "D." These six features combined with the basic A, B, and C features and classified by TDS and the other six classification algorithms. It was noted that the high accuracy was achieved by classifying the ABCD features related to automatic ANN and was 98.75%.

Regarding the results observed above, it was quite noticeable that the twenty-four features represented by ABCD whether by using different calculation methods for "D" yielded high accuracy but with rare variations. Geometric features representing "D" showed perfect accuracy when classifying data by linear SVM upon clinical images. Also, linear SVM reached the best accuracy at classifying data by using the differential structure for dermoscopic images. The classification results of ABCD are very promising to define melanoma for both dermoscopic and clinical images.

Accordingly, it could be concluded that the ABCD model gives a good representation for the PSL that it records the perfect results whatever it is applied upon dermoscopic or clinical databases. Figures 16 and 17 show the bar chart of the results achieved by all approaches performed on both dermoscopic and clinical images database, respectively.

6 Conclusions

This study presents a new method for detecting the lesion differential structure using the different color spaces HSV, YCbCr, and Lab. Also, spectral analysis was introduced for the aim of filtration in some structures. As a result of the seven different methods

used for classification and the three different procedures used to define the "D" parameter, twenty-one different experiments were operated on dermoscopic images and fourteen on clinical images. The proposed experiments show very promising results for both databases. For the dermoscopic database ABCD model represented by geometric, texture features and differential structures for parameter "D" showed the best accuracy 98.1% by TDS, 95% by Automatic ANN, and 98.75 by linear SVM, respectively. For clinical database ABCD model represented by geometric and texture features for parameter "D" showed a perfect accuracy of 100% when classified by linear SVM and 98.75% when classified by automatic ANN. Finally, the whole system was presented in a GUI form.

References

1. Navarrete-Dechent C, Dusza SW, Liopyris K, Marghoob AA, Halpern AC, Marchetti MA (2018) Automated dermatological diagnosis: hype or reality? J Invest Dermatol 138(10):2277–2279
2. Jerant A, Johnson J, Sheridan C, Caffrey T (2000) Early detection and treatment of skin cancer. Am Fam Physician 62(2):357–386
3. Markovic S, Erickson L, Rao R, McWilliams R, Kottschade L, Creagan E et al (2007) Malignant melanoma in the 21st century. Part 1: Epidemiology, risk factors, screening, prevention, and diagnosis. Mayo Clin Proc 82(3):364–380
4. Yang J, Sun X, Liang J, Rosin PL (2018) Clinical skin lesion diagnosis using representations inspired by dermatologist criteria. In Proceedings of the IEEE Conference on Computer Vision and Pattern Recognition, pp. 1258–1266
5. Nachbar F, Stolz W, Merkle T, Cognetta AB, Vogt T, Landthaler M, Bilek P, Braun-Falco O, Plewig G (1994) The ABCD rule of dermatoscopy: high prospective value in the diagnosis of doubtful melanocytic skin lesions. J Am Acad Dermatol 30(4):551–559
6. Fabbrocini G, Betta G, Di Leo G, Liguori C, Paolillo A, Pietrosanto A et al (2010) Epiluminescence image processing for melanocytic skin lesion diagnosis based on 7-point check-list: a preliminary discussion on three parameters. Open Dermatol J 4(1):110–115
7. Abder-Rahman AA, Deserno TM (2012) A systematic review of automated melanoma detection in dermatoscopic images and its ground truth data. In: Proc. SPIE 8318, Medical Imaging: Image Perception, Observer Performance, and Technology Assessment
8. Stoecker WV, Moss RH (1992) Editorial: digital imaging in dermatology. Comput Med Imaging Graph 16(3):145–150
9. Ganster H, Pinz A, Röhrer R et al (2001) Automated melanoma recognition. IEEE Trans Med Imaging 20:233–239
10. Blum A, Rassner G, Garbe C (2003) Modified abc-point list of dermoscopy: a simplified and highly accurate dermoscopic algorithm for the diagnosis of cutaneous melanocytic lesions. J Am Acad Dermatol 48(5):672–678
11. Blum A, Luedtke H et al (2004) Digital image analysis for diagnosis of cutaneous melanoma. Development of a highly effective computer algorithm based on analysis of 837 melanocytic lesions. Br J Dermatol 151:1029–1038
12. Amaliah B, Fatichah C, Widyanto MR ABCD feature extraction for melanoma skin cancer diagnosis The International Conference on Advanced Computer Science and Information Systems (ICACCIS 2009)
13. Sheha MA, Mabrouk MS, Sharawy A (2013) Automatic detection of melanoma skin cancer using texture analysis. Int J Comput Appl 42(20):22–26
14. Mabrouk MS, Sheha MA, Sharawy AA (2013) Computer aided diagnosis of melanoma skin cancer using clinical photographic images. Int J Comput Technol 10(8):1922–1929
15. Ramteke NS, Jain SV (2013) ABCD rule based automatic computer-aided skin cancer detection using MATLAB. Int J Comput Technol Appl 4(4):691–697
16. Sheha MA, Mabrouk MS, Sharawy AA (2014) Pigmented skin lesion diagnosis using geometric and chromatic features, Biomedical Engineering Conference (CIBEC), Cairo International, IEEE

17. Jaina S, Jagtapb V, Pise N (2014) Computer aided melanoma skin cancer detection using image processing. International Conference on Intelligent Computing, Communication & Convergence (ICCC-2014), Conference Organized by Interscience Institute of Management and Technology
18. Sheha MA, Mabrouk MS, Sharawy AA (2016) Automated imaging system for pigmented skin lesion diagnosis. (IJACSA) Int J Adv Comput Sci Appl 7(10)
19. Sachdeva N, Gupta R (2017) Hybrid approach to investigate the probability of skin cancer by ABCD and PCA method. Int J Adv Res Electron Commun Eng (IJARECE) 6(4)
20. Ali A-RA, Deserno TM (2012) A systematic review of automated melanoma detection in dermatoscopic images and its ground truth data. Department of Medical Informatics, Aachen University of Technology (RWTH), 52057 Aachen, Germany
21. Maglogiannis I, Doukas N (2009) Overview of advanced computer vision systems for skin lesions characterization. IEEE Trans Inf Technol Biomed 13(5)
22. Hoshyar AN, Al-Jumaily A, Sulaiman R (2011) Review on automatic early skin cancer detection. 978–1–4244-9763-8/11/$26.00 ©2011 IEEE
23. Dorj U-O, Lee K-K, Choi J-Y, Lee M (2018) The skin cancer classification using deep convolutional neural network. Multimed Tools Appl 77:9909–9924
24. Esteva A, Kuprel B, Novoa RA, Ko J, Swetter SM, Blau HM, Thrun S (2017) Dermatologist-level classification of skin cancer with deep neural networks. Nature 542(7639):115–118
25. Korotkov K, Garcia R (2012) Computerized analysis of pigmented skin lesions: a review. Artif Intell Med 56(2):69–90
26. Blum A, Luedtke H, Ellwanger U, Schwabe R, Rassner G, Garbe C (2004) Digital image analysis for diagnosis of cutaneous melanoma. Development of a highly effective computer algorithm based on analysis of 837 melanocytic lesions. BJD 151:1029–1038
27. Zapirain BG, Zorrilla AM, Oleagordia IR, Nunez G, Abtane A (2009) Skin cancer parameterization algorithm based on epiluminiscence image processing, IEEE
28. Ruiz D, Berenguer V, Soriano A, Sánchez B (2011) A decision support system for the diagnosis of melanoma: a comparative approach
29. Holmström T-B, Georgsson F. A survey and evaluation of features for the diagnosis of malignant melanoma, Master thesis in Computing Science
30. Lee TK, McLean DI, Atkins MS (2003) Irregularity index. A new border irregularity measure for cutaneous melanocytic lesions. Med Image Anal 7:47–64
31. Johr R, Soyer HP, Argenziano G, Hofmann-Wellenhof R, Scalvenzi M (2004) Dermoscopy the essentials. Mosby
32. Masood A, Al-Jumaily AA (2013) Computer aided diagnostic support system for skin cancer: a review of techniques and algorithms. Int J Biomed Imaging 323268
33. Grammatikopoulos G, Hatzigaidas A, Papastergiou A, Lazaridis P, Zaharis Z, Kampitaki D, Tryfon G (2006) Automated malignant melanoma detection using MATLAB", Proceedings Of The 5th Wseas Int. Conf. On Data Networks, Communications & Computers, Bucharest, Romania, October 16-17, 2006
34. Alcón JF, Ciuhu C, ten Kate W, Heinrich A, Uzunbajakava N, Krekels G, Siem D, de Haan G (2009) Automatic imaging system with decision support for inspection of pigmented skin lesions and melanoma diagnosis. IEEE J Select Topics Sign Process 3(1)
35. Peeters M, Neyens J, Geerts S, Ledda A (2010) Computer image analysis of pigmented skin lesions, Bachelor's thesis
36. Fleming MG, Steger C, Zhang J, Gao J, Cognetta AB, Pollak I, Dyer CR (1998) Techniques for a structural analysis of dermatoscopic imagery. Comput Med Imaging Graph 22:375–389
37. Di Leo G, Paolillo A, Sommella P, Fabbrocini G (2010) Automatic diagnosis of melanoma: a software system based on the 7-point check-list. Proceedings of the 43rd Hawaii International Conference on System Sciences
38. Huertas Fernández I, Caiani E (2011) Computer-aided detection and classification of pigment network in pigmented skin lesions. Politecnico, Di Milano
39. Sáez A, Acha B, Serrano C (2014) Pattern analysis in dermoscopic images, Computer vision techniques for the diagnosis of skin Cancer. Ser BioEng. https://doi.org/10.1007/978-3-642-39608-3_2
40. Anantha M, Moss RH, Stoecker WV (2004) Detection of pigment network in dermatoscopy images using texture analysis. Comp Med Imaging Graph 28(5):225–234
41. Hart PE, Stork DG, Duda RO (2000) Pattern classification, 2nd edn. John Wiley & Sons, Hoboken
42. Scholkopf B, Kah-Kay S, Burges CJ, Girosi F, Niyogi P, Poggio T, Vapnik V (1997) Comparing support vector machines with Gaussian kernels to radial basis function classifiers. IEEE Trans Sign Process 45: 2758–2765

43. Mohd A, Ram GK, Shafeeq A (2017) Skin cancer classification using K-means clustering. Int J Tech Res Appl 5(1):62–65
44. Russakovsky O et al (2015) Imagenet large scale visual recognition challenge. Int J Comput Vis 115: 211–252
45. Isasi AG, Zapirain GB, Zorrilla MA (2001) Melanomas non-invasive diagnosis application based on the ABCD rule and pattern recognition image processing algorithms. Comput Biol Med 41:742–755

Affiliations

Mai S. Mabrouk[1] · Ahmed Y. Sayed[2] · Heba M. Afifi[3] · Mariam A. Sheha[4] · Amr Sharwy[4]

✉ Mai S. Mabrouk
msm_eng@yahoo.com

[1] Biomedical Engineering Department, MisS University for Science and Technology (MUST University), Giza, Egypt

[2] Department of Engineering Mathematics and Physics, El- Mataria, Helwan University, Cairo, Egypt

[3] Bioelectronics Engineering Department, Modern University for Technology and Information (MTI University), Cairo, Egypt

[4] Biomedical and System Engineering Department, Cairo University, Giza, Egypt